^{3}He melting-curve thermometry at millikelvin temperatures

Dennis S. Greywall
AT&T Bell Laboratories, Murray Hill, New Jersey 07974
(Received 2 August 1984)

A pressure-versus-temperature calibration of the ^{3}He melting curve is given for $1 < T < 250$ mK. The calibration is based on the data of Halperin *et al.* and Greywall and Busch and is consistent with the revised National Bureau of Standards temperature scale. On the new scale, $T_A = 2.708$ mK. With the use of the transition line between normal and superfluid ^{3}He [i.e., $T_c(P)$] as a basis for intercomparison, the melting-curve scale is found to be proportional to the magnetic temperature scales of Paulson *et al.* and Haavasoja *et al.* Included is a description of the $PrNi_5$ nuclear demagnetization refrigerator which was used to cool the ^{3}He samples to less than 0.3 mK.

I. INTRODUCTION

The melting curve (MC) of ^{3}He, as a continuous set of pressure-temperature fixed points, provides a precise thermometry standard which extends down in temperature to below 1 mK. Certainly this has been known for a long time,[1] yet the unique potential of this standard has not been fully exploited. Recently, via specific-heat[2] and thermal-conductivity[3] measurements on normal liquid ^{3}He, it was demonstrated that MC thermometry[4] is a viable and important alternative to other types of low-temperature thermometry, and that it need not be relegated only to experiments performed on the melting curve itself. However, it is at even lower temperatures, that is, at temperatures of less than a few millikelvin, where the ^{3}He melting curve (because of the lack of better alternatives) becomes indispensable as a precise standard. At these very low temperatures, the device sensing the melting pressure can be used either as a continuous thermometer or simply, and perhaps even more importantly, as an accurate detector of the two superfluid transitions in the liquid phase and the magnetic transition in the solid phase. These three special fixed points are independent of pressure-gauge calibration and are analogous to the superconducting fixed points used at much higher temperatures.

In this paper we discuss the detection of the three special fixed points and the assignment of temperature values to these transitions. An empirical relation is provided which describes the melting curve between 1 and 250 mK. This calibration is consistent with the revised National Bureau of Standards (NBS) (CTS-1983) temperature scale[5] and the adjusted P-T melting-curve data of Greywall and Busch[4] above 15 mK, and with the renormalized P-T measurements of Halperin *et al.*[6] at lower temperatures. Using this MC scale we give the coordinates of the transition line between normal and superfluid ^{3}He, and make a comparison with other determinations. We begin by describing our nuclear demagnetization cryostat.

II. EXPERIMENTAL DETAILS

A. Nuclear demagnetization refrigerator

Figure 1 shows the cryostat below the level of the mixing chamber of the dilution refrigerator. An unusual feature of the cryostat is the location of the 5-T superconducting magnet inside the evacuated 4-K shield and the attachment of the magnet to the 1-K refrigerator. This arrangement greatly simplified the modifications necessary to incorporate the modular and compact nuclear refrigerator into our existing apparatus.

The nuclear coolant is 0.64 moles of $PrNi_5$ (Ref. 7) in the form of seven 8-mm-diam hexagonal rods, each 9.5 cm long. The rods were ground to this shape, beginning

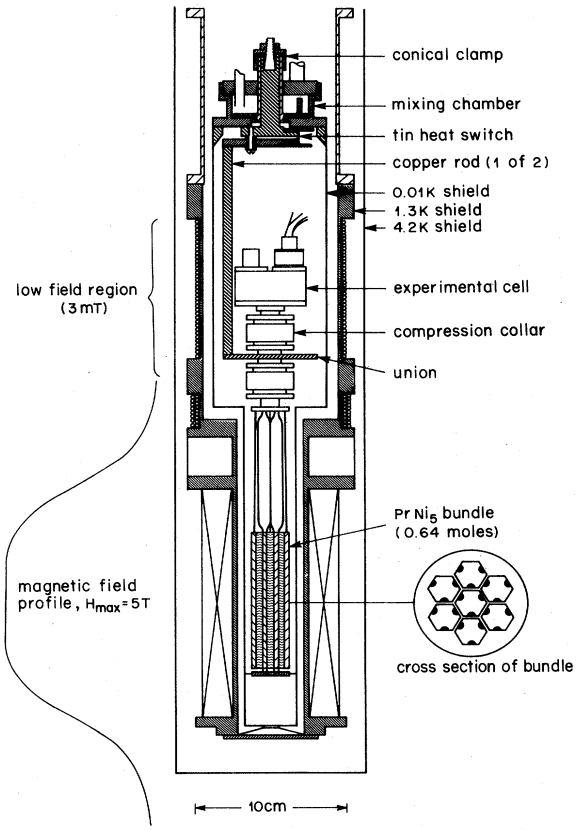

FIG. 1. Nuclear demagnetization refrigerator.

with ingots cast with three of the adjacent long flat faces. In alternate faces, grooves of semicircular cross section (1.5 mm diam) were ground the length of the rods. Annealed, high-purity copper wires[8] were cadmium-soldered into these grooves. Before the annealing and soldering operations, the copper wires (1.25 mm diam) were pressed (using steel forms) to have a cross section that closely matched the grooves (see the inset of Fig. 1). After soldering, the rods were cleaned and lightly sand-blasted and electroplated with approximately 0.07 mm of copper[9] to improve the thermal contact between the copper wires and the $PrNi_5$ rods. The seven rods were then tied into a compact bundle and the free ends of the wires welded[10] to an annealed copper flange. Machined as part of this flange is a 3.2-cm-long by 1.3-cm-diam post, to which mechanical and thermal connection is made. In an attempt to reduce eddy-current heating caused by the radial component of the magnetic field[11] the three wires attached to each rod were bent so that over most of their free length (10 cm) they were in the same radial plane. The wires on the central rod were pushed close to the axis. Bands of epoxy-covered thread maintain a spacing between rods of about 0.5 mm. Two bands of thread are also used to hold the bundle of rods rigidly together.

Thermal contact between the post on the bundle assembly and the experimental cell is made via a copper union which employs a pair of compression collars.[12] These collars make use of the small expansion coefficient of tungsten and tighten around the close-fitting (gold-plated) cylindrical copper pieces with decreasing temperature. Two 0.64-cm-diam copper rods welded to the flange machined as part of the union support the union. At their upper ends the copper rods were welded to the lower of a pair of copper plates separated by four 2.5-mm-thick Vespel[13] spacers. The upper plate is in good thermal contact with the mixing chamber of a dilution refrigerator via a low-resistance conical clamp. The two plates are bridged by a superconducting heat switch cut from a 0.8-mm-thick piece of high-purity tin. The butterfly-shaped piece has a width at its neck of about 2 mm and an electrical resistivity ratio of about 3000.[14]

The nuclear stage is surrounded by a radiation shield attached to the mixing chamber of the dilution refrigerator. The large-diameter section (see Fig. 1) of the shield is copper; the lower, smaller-diameter section is brass with a slit running most of its length. Vibrational motion of the shield relative to the magnet is reduced using thread tie-downs. The $PrNi_5$ bundle is quite rigidly positioned inside the mixing chamber shield via a spider attached to the bottom of the bundle. The spider is made from a disk of Vespel[13] and has three fingers of looped phosphor bronze wire.

Some more technical details follow: The (300—4)-K electrical resistivity ratio measured for one of the $PrNi_5$ rods along its full length is 21. The ratio measured on a sliver cut from near the end and perpendicular to the axis of another rod is 49. The difference in these values is presumably related to the visible cracking in each of the rods perpendicular to its axis. Since the heat flow is primarily in the radial direction, the larger number is the more meaningful.

The copper wires[8] used for the link to the bundle had a resistivity ratio of 1350 after annealing. However, to straighten the wires and to improve their mechanical properties the wires were stretched[15] by 2%, thereby reducing the ratio to 1050. The low-temperature electrical resistance of the 21 wires in parallel, between the middle of the bundle and the weld to the flange, is 90 nΩ. The electrical resistance between the coolant and the union platform (Fig. 1), determined from thermal measurements performed near 1 mK, is 140 nΩ. The difference between these numbers includes the resistance of one press joint, the welds, and the resistance of the $PrNi_5$ itself. (Converting the 140 nΩ to thermal resistance, we have $R^{\rm th}=5.6/T$ measured in units of K/W. At 1 mK, a 1-nW heat leak will generate a temperature difference between the union and the bundle of 5.6 μK.) The electrical resistance measured between the mixing chamber and the union is 0.5 μΩ.

The time for precooling the nuclear stage in a 4-T field is 4 h to 30 mK, 12 h to 20 mK, and 30 h to 10 mK. The usual procedure is to let the system cool overnight and begin the demagnetization at a starting temperature between 12 and 14 mK. The temperature is reduced to T_A in about 1 h with little loss of entropy. The magnetic field is then dropped at considerably slower rates. The lowest temperature reached is ≤ 0.3 mK, measured using a melting-curve thermometer. After a few weeks of operation, the heat leak is about 1 nW.

B. ^{3}He cell

The cylindrical, ^{3}He sample cell is shown in Fig. 2. It is made mainly of copper and has an open volume of about 12 cm^3. The cap threads onto the base and is sealed with epoxy. The two short towers are sealed to the cap using indium o-rings. One tower is lead-plated on the inside and contains a lanthanum-diluted cerium magnesium nitrate (LCMN) thermometer.[16] The second holds a vibrating-wire viscometer, which, however, was not used for the work described in this paper. The sintered-silver heat exchanger was made using 28 g of 700-Å silver powder,[17] and has a surface area[18] of about 70 m^2. Thermal contact between the sinter and the cell body is

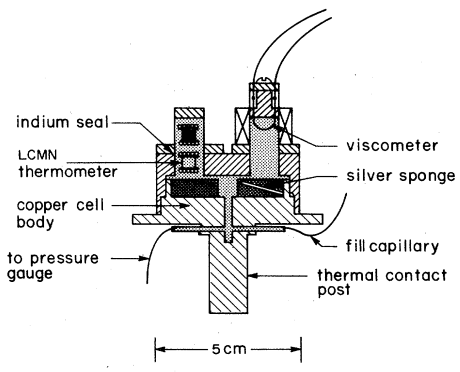

FIG. 2. Experimental cell.

via 36, 1.2-mm-diam, silver-plated, high-purity copper wires which were soldered[19] into holes drilled radially into the cell base tangent to the bottom of the main cavity. As discussed in the preceding subsection, thermal contact between the cell and the $PrNi_5$ assembly is via mechanical clamps. The fill line between the cell and the mixing chamber is a 1-m length of 0.008-cm-i.d. CuNi capillary. A second 5-cm length of capillary connects the cell to a pressure gauge mounted on the union flange. This gauge is identical to the melting-curve thermometer also mounted on the union. A drawing of the gauges is shown in Fig. 1 of Ref. 4.

C. Pressure-gauge calibrations

The melting-curve thermometer and sample pressure gauge were pressure-calibrated against a gas-lubricated deadweight tester. The melting-curve—thermometer calibration was performed at 1 K in the range from 28 to 35 bars and the capacitance-versus-pressure results were fitted using the expression

$$P=\sum_{l=0}^{4} a_l (1/C)^l . \tag{1}$$

The rms deviation is 0.12 mbar. Since the fill line to this gauge passes through the bath in an evacuated jacket, the hydrostatic-pressure-head correction is small and estimated to be 2 mbar. The capacitance of the gauge was measured using a simple ratio transformer bridge circuit with the reference fixed capacitor, shown in Fig. 3, also mounted on the union. With a bridge excitation voltage of 2 V rms, the pressure resolution of the gauge was 3 μbar at 34 bars.

The sample pressure gauge was calibrated between 0 and 35 bars during the actual course of the experiment with the sample temperature near 5 mK. These capacitance-versus-pressure values were fitted using the equation

$$P=\sum_{l=0}^{4} b_l (1/C_0-1/C)^l . \tag{2}$$

The quantity C_0 is the capacitance measured at $P=0$. The rms deviation of this fit was 0.005%. From a comparison of the apparent pressure measured at the minimum in the melting curve with the corresponding pressure determined using the melting-curve thermometer, it was determined that the hydrostatic head correction was 12.5 mbar.

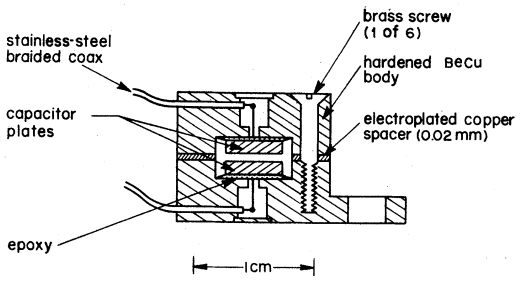

FIG. 3. Reference capacitor, 20 pF.

III. RESULTS AND DISCUSSION

A. Special features on the melting curve

There are several special features along the melting curve of ^{3}He which are easily detected using a melting-curve thermometer and which provide an indispensable, precise set of very-low-temperature fixed points. These are, of course, (i) the second-order transition between the normal liquid and the superfluid A phase (at T_A), (ii) the first-order transition between the B and A superfluid phases (at T_{BA}), and (iii) the first-order transition of solid ^{3}He into the antiferromagnetically ordered phase (at T_S). It should be noted that the precise detection of these three fixed points is not at all dependent on having an accurate pressure calibration of the melting curve thermometer. It becomes necessary to have an accurate pressure calibration though to take advantage of the entire melting curve, which provides a continuous set of low-temperature fixed points. This pressure calibration, however, can be performed quite easily using the known pressures of the special fixed points. These pressures are listed in Table I, in which a comparison is made with previous measurements.[6,20,21] All of the values agree extremely well. Only the values of $P_A-P_{\min}$ are outside of combined uncertainties. $P_{\min}$ is the pressure at the minimum in the melting curve. Note that ^{4}He impurities will depress the minimum in the melting curve, but, because of phase separation, should have little effect at very low temperature. The ^{3}He sample we used had less than 2 ppm ^{4}He.

Tracings of the melting pressure versus time, recorded in the vicinity of each of the transitions, are shown in Figs. 4(a)—4(c). For each tracing the temperature is slowly warming (i.e., the melting pressure is slowly decreasing).

Some observations about each of the transitions follow: The A transition is second order and there is no latent heat; therefore, according to the Clausius-Clapeyron equation, there can be no change in the slope of the melting curve at T_A. Figure 4(c) shows an obvious kink at T_A which is present only because the system is drifting and is not in thermal equilibrium. It reflects the large changes in the thermodynamic properties of the liquid at T_A. As the drift rate is reduced, the transition should become pro-

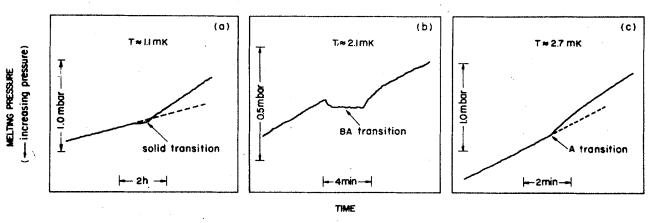

FIG. 4. Special features on the melting curve of ^{3}He. The tracings show melting pressure vs time recorded with the system warming slowly.

TABLE I. Measured pressures of the special features on the melting curve of ^{3}He.

	P_{min} (bars)	P_A (bars)	P_{BA} (bars)	P_S (bars)	P_A-P_{min} (mbar)	$P_{BA}-P_A$ (mbar)	P_S-P_A (mbar)
This work	29.3175 ±0.003	34.3380 ±0.003	34.3580 ±0.003	34.3905 ±0.003	5020.5 ±1.0	20.00 ±0.03	52.52 ±0.10
Halperin *et al.*	29.3160 ±0.003	34.3420 ±0.003	34.3619 ±0.003	34.3943 ±0.003	5026.0 ±1.0	19.90 ±0.10	52.3 ±0.2
Avenel *et al.*		34.348	34.368	34.400		20.0	52.1
Kobiela *et al.*					5029.5	19.96 ±0.10	52.4 ±0.2

gressively more difficult to detect. In practice, we found that, even at rates an order of magnitude slower than that shown in Fig. 4(c), the transition was easily detected. P_A did not change with drift rate, and there was little difference in P_A values determined upon warming and cooling. When drifting up and down at 0.2 mbar/min, the two P_A values were the same within 10 μbar ($\sim$0.3 μK).

The obvious feature of the B-A transition shown in Fig. 4(b) is the region of constant temperature. This flat in the warming curve, along with the transient superheating, are clear indicators that the transition is first order. There should also then be a change in the slope of the melting curve, but the latent heat[6] is very small and the change is only a few tenths of a percent. Superheating of the transition was never a serious problem. In fact, by slowing the warming rate the amount of superheating could be reduced to a nearly undetectable level. In contrast to this, the supercooling of the transition was always quite appreciable. Although the precise amount of supercooling must depend on a number of variables, we observed that for our device the amount of supercooling was always very close to 0.29 mK. Obviously, to be used as a fixed point, measurements must be made upon warming.

The solid transition, Fig. 4(a), is also first order, but in many respects the character of this transition, as observed using a melting-curve thermometer, is very different from the B-A transition in the liquid. There is a very large latent heat involved[22] which manifests itself through the fact that the slope of the melting curve changes by a factor of about 3.5. This makes this transition extremely easy to detect, even when cooling or warming extremely fast. Another virtue of this fixed point is that there appears to be little if any superheating or supercooling. Figure 4(a) shows quite a slow sweep through the transition, but covering the same temperature range in $\sim$20 min gave the same P_S to within the precision of the measurement.

B. Temperatures of the ^{3}He transitions

In recent years many very different thermometry techniques have been employed to assign temperatures to the ^{3}He transitions.[23,24] The values for the A transition are generally in the range 2.6 to 2.8 mK, the B-A values between 2.06 and 2.20 mK, and the solid transition temperatures between 1.03 and 1.10 mK. Although each type of thermometry used has its special virtues and advantages, all, at least at the present time, are purported to have errors of roughly the same magnitude, and one scale cannot be singled out *a priori* as being the most accurate. We have chosen, though, to tie our results to the Cornell thermodynamic scale,[6] which is generated using the ^{3}He melting curve itself. The real advantage of this scale is that it is based strictly on thermodynamic measurements. Consequently, and contrary to the other methods, there is no physical relation involved whose adequacy for accurately defining temperature can be questioned. This also means that unambiguous and meaningful estimates of the uncertainties in this scale can be made. Moreover, since ^{3}He is the thermometry substance, sample impurities are not a serious problem.

The procedure used at Cornell was to hold the temperature fixed (i.e., melting pressure) and then to measure the volume change resulting from the injection of a known amount of heat into the liquid-solid mixture. This information and the Clausius-Clapeyron equation permitted Halperin *et al.*[6] to relate T/T_A to P-P_A. Then using the condition that the solid (nuclear-spin) entropy be R ln2 at temperatures large compared to T_S, they determined $T_A=(2.75\pm0.11)$ mK. On this scale, $T_{BA}=(2.18\pm0.10)$ mK and $T_S=(1.10\pm0.06)$ mK.

We choose now to renormalize this scale slightly in order to force the Cornell scale to coincide with the NBS-CTS-1983 scale at the superconducting transition of tungsten (W). This also permits a smooth tie onto the high-temperature melting-curve calibration (Sec. III D). Combining our measurement of P_A-P_W (518.1 mbar) and the NBS T_c for tungsten (15.57 mK) with the results of Halperin *et al.*, we find $T_A=2.708$ mK, $T_{BA}=2.138$ mK, and $T_S=1.082$ mK. The uncertainties in these temperatures remain the same as in the original Cornell values.

C. T_c of tungsten

In this section we digress and make some brief comments about the changing values for the T_c of tungsten.

Recently, we reported a T_c for tungsten of 15.74 mK

and compared this with the originally assigned NBS value, 15.14 mK. Our temperature was determined using a CMN thermometer calibrated against the NBS fixed points at nominal temperatures of 100, 160, and 200 mK. The CMN Δ [$\chi \propto 1/(T-\Delta)$] was taken to be that which yielded a linear low-temperature specific heat for normal ^{3}He.

More recently, the NBS revised the T_c values for the three higher-temperature fixed points downward by approximately 0.5% (which is within the estimated uncertainty of the original temperatures). Using these corrected temperatures, a reanalysis of the C_V data yielded a tungsten T_c of 15.66 mK. The revised NBS T_c for tungsten (which is the same for all of the NBS samples) is 15.57 mK. The two T_c(W) values now agree to within 0.6%, which is within the combined experimental uncertainties.

D. Empirical equation for the ^{3}He melting curve

The expression

$$P-P_A=\sum_{l=-3}^{5} a_l T^l , \tag{3}$$

with

$$a_{-3}=-0.260\,784\,92\times10^{-1} ,$$
$$a_{-2}=0.843\,248\,81\times10^{-1} ,$$
$$a_{-1}=-0.109\,908\,60 ,$$
$$a_0=0.151\,204\,00 ,$$
$$a_1=-0.450\,703\,32\times10^{-1} ,$$
$$a_2=0.173\,702\,24\times10^{-3} ,$$
$$a_3=-0.521\,411\,83\times10^{-6} ,$$
$$a_4=0.125\,616\,45\times10^{-8} ,$$
$$a_5=-0.140\,515\,00\times10^{-11} ,$$

describes the ^{3}He melting curve between 1 and 250 mK. Pressure and temperature are measured in bars and millikelvin, respectively. The relative deviations from this weighted $(1/T^2)$ least-squares fit of the data are shown in Fig. 5. The open circles are the data of Halperin *et al.*[20] based on a T_A value of 2.708 mK (Sec. III B). The solid circles at higher temperatures are the data from Ref. 4 corrected to account for the revisions in the NBS temperature scale (Sec. III C). The temperature measurements in Ref. 4 were made using a simple CMN ratio transformer bridge circuit. The bridge ratio R is related to the temperature by $1/(T-\Delta)=\alpha X+\beta$, where $X=R/(1-R)$. In the reanalysis of the data, the three parameters Δ, α, and β were determined[25] using the NBS-CTS-1983 transition temperatures for W (15.57 mK), Ir (98.65 mK), and $AuIn_2$ (204.80 mK). A check of the calibration was made using the $AuAl_2$ (161.92 mK) transition where the two temperatures agreed to within 0.025%. Unfortunately, a similar check could not be made using the T_c for Be since our sample had an extremely broad transition and was not recalibrated on the revised NBS scale. The P-T data from Ref. 4 between 7 and 15 mK were not included in the fit since they were obtained using an LCMN thermometer, and the Δ for this device was not accurately determined. Presumably, the systematic deviations seen in Fig. 5, of the order of a few tenths of a percent, are due mainly to the inadequacy of the fitting function, but they may also indicate small errors in the measurements themselves. A list of smooth pressure-temperature values is given in Table II.

Figure 6 shows $|(1/T)(dT/dP)|$ computed using Eq. (3). This quantity, multiplied by the pressure resolution of a particular melting-curve thermometer, gives the relative temperature resolution. For example, if the device has a pressure resolution of 10 μbar, the precision of the temperature measurements is 3 parts in 10^4 at 1 mK, 3 parts in 10^5 at 10 mK, and 5 parts in 10^6 at 100 mK.

The relative differences between the new melting-curve calibration defined by Eq. (3) and that used in recent experiments to measure the specific heat[2] and thermal conductivity[3] of normal ^{3}He is plotted in Fig. 7. Over the entire range in which the C_V and κ measurements were

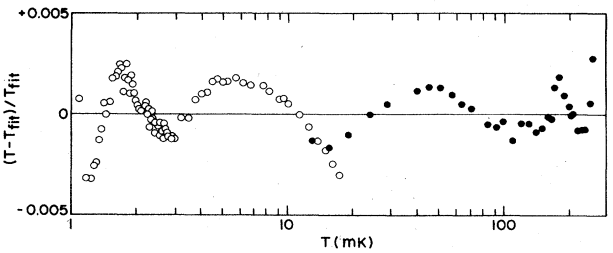

FIG. 5. ^{3}He-melting-curve data plotted as relative temperature deviations from Eq. (3). The open circles are the data of Halperin *et al.* (Ref. 5) using $T_A=2.708$ mK. The solid circles are the results of Greywall and Busch (Ref. 4) corrected to account for revisions in the NBS temperature scale.

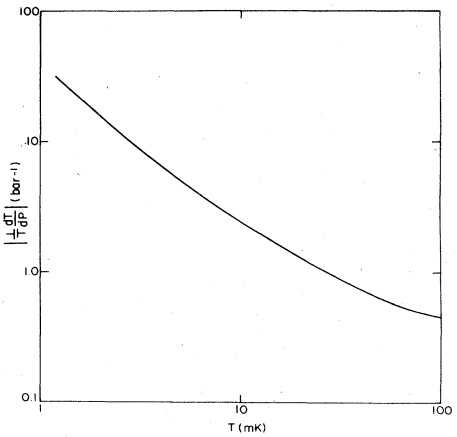

FIG. 6. $|(1/T)(dT/dP)|$ along the ^{3}He melting curve determined using Eq. (3). This quantity multiplied by the pressure resolution of a particular melting-curve thermometer gives the relative temperature resolution of the device.

TABLE II. ^{3}He-melting-curve coordinates determined using Eq. (3).

T (mK)	$P-P_A$ (bars)	dP/dT (bars K^{-1})	T (mK)	$P-P_A$ (bars)	dP/dT (bars K^{-1})	T (mK)	$P-P_A$ (bars)	dP/dT (bars K^{-1})
1.081(T_s)	0.05252	−26.9	4.0	−0.0489	−39.2	75.0	−2.4370	−25.9
1.1	0.0520	−27.1	5.0	−0.0887	−40.2	80.0	−2.5642	−25.0
1.2	0.0492	−28.2	6.0	−0.1292	−40.7	85.0	−2.6869	−24.1
1.3	0.0464	−29.0	7.0	−0.1700	−40.9	90.0	−2.8053	−23.3
1.4	0.0435	−29.6	8.0	−0.2110	−41.0	95.0	−2.9196	−22.4
1.5	0.0405	−30.2	9.0	−0.2519	−40.9	100.0	−3.0297	−21.6
1.6	0.0374	−30.8	10.0	−0.2928	−40.8	110.0	−3.2384	−20.1
1.7	0.0343	−31.4	11.0	−0.3335	−40.6	120.0	−3.4323	−18.7
1.8	0.0311	−32.0	12.0	−0.3741	−40.4	130.0	−3.6122	−17.3
1.9	0.0279	−32.6	14.0	−0.4545	−40.0	140.0	−3.7786	−16.0
2.0	0.0246	−33.1	16.0	−0.5341	−39.5	150.0	−3.9323	−14.7
2.1	0.0213	−33.6	18.0	−0.6125	−39.0	160.0	−4.0738	−13.5
2.138(T_{BA})	0.02000	−33.8	20.0	−0.6900	−38.5	170.0	−4.2034	−12.4
2.2	0.0179	−34.1	25.0	−0.8789	−37.1	180.0	−4.3218	−11.3
2.3	0.0145	−34.6	30.0	−1.0612	−35.8	190.0	−4.4293	−10.2
2.4	0.0110	−35.0	35.0	−1.2371	−34.5	200.0	−4.5264	−9.2
2.5	0.0075	−35.4	40.0	−1.4067	−33.3	210.0	−4.6135	−8.2
2.6	0.0039	−35.8	45.0	−1.5702	−32.1	220.0	−4.6911	−7.3
2.7	0.0003	−36.2	50.0	−1.7280	−31.0	230.0	−4.7598	−6.4
2.709(T_A)	0.00000	−36.2	55.0	−1.8801	−29.9	240.0	−4.8201	−5.6
2.8	−0.0033	−36.5	60.0	−2.0269	−28.8	250.0	−4.8728	−4.9
2.9	−0.0070	−36.8	65.0	−2.1685	−27.8			
3.0	−0.0107	−37.1	70.0	−2.3052	−26.8			

made, the difference is less than 1%. For $T \geq 70$ mK the difference is quite uniformly 0.5%. The implied modifications to the low-temperature specific-heat results are shown in Fig. 8 where C_V/RT at 0.06 bar is plotted using both the new (solid circles) and old (open circles) temperature scales. Conversion of the C_V data was made using the relation

$$\left[\frac{C_V}{T}\right]_{\text{new}} = \left[\frac{C_V}{T}\right]_{\text{old}} \left[\frac{1}{T}\frac{dP}{dT}\right]_{\text{new}} \Big/ \left[\frac{1}{T}\frac{dP}{dT}\right]_{\text{old}} . \quad (4)$$

Note that both strings of data in Fig. 8 are consistent with a normal ^{3}He specific heat that is tending toward a linear temperature dependence at low temperatures. In Ref. 2 this condition was imposed on the data and was used as an input in determining the (old) temperature scale. The condition of a linear, low-temperature specific heat is now being used only as a check on the new temperature scale. Another check can be made by using the revised C_V data to compute the entropy of the liquid at the minimum in the melting curve. Here the liquid and solid entropies are equal, and it is known that the solid entropy is due mainly to the nuclear spins plus a very small contribution from the phonons. The computed liquid entropy is $1.008R$ ln2, in excellent agreement with the expected results.

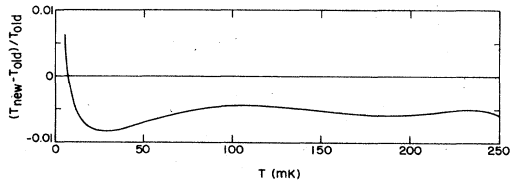

FIG. 7. Relative difference between the melting-curve calibration given by Eq. (3) and that used in Refs. 2 and 3.

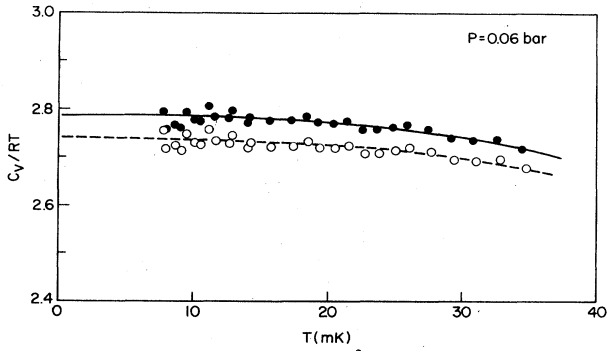

FIG. 8. Specific heat of normal ^{3}He based on the melting-curve calibration given by Eq. (3) (solid circles) and on the calibration given in Ref. 2 (open circles).

E. Superfluid phase diagram

The pressure-temperature boundary between the normal and superfluid phases of liquid ^{3}He [i.e., $T_c(P)$] provides like the melting curve, a continuous set of low-temperature fixed points. Here, though, the temperature range is limited to between roughly 1 and 2.7 mK. Nonetheless, for those working on superfluid ^{3}He the transition line is the natural reference for intercomparing temperature scales. In this section we relate the pressure-temperature coordinates of the superfluid phase boundary to those of the melting curve.

The superfluid transition off of the melting curve was detected using the LCMN thermometer located inside the experiment cell (Fig. 2). At the transition the LCMN thermometer tracing shows a kink similar to that observed with the melting-curve thermometer at T_A [Fig. 4(c)]. The procedure followed, for low sample pressures, was simply to drift up and down in temperature very slowly and to record the melting-curve—thermometer readings and also the sample pressure at the transition indicated by the LCMN thermometer. The melting-curve—thermometer readings obtained upon warming and cooling differed typically by ~ 0.1 mbar (4 μK), and the averaged reading was used. As the pressure was increased, however, it was necessary, because of the decreasing thermal diffusivity[3] and increasing boundary resistance,[26] to drift at slower and slower rates. Above 11 bars the data-taking procedure was modified. For these higher pressures, pairs of LCMN and melting-curve bridge readings were recorded first with the temperature stabilized slightly below and then slightly above T_c. The melting-curve—thermometer reading at T_c was determined by interpolation using these calibration pairs, and the LCMN reading at T_c obtained from a slow drift through the transition.

The data, consisting of the sample pressure P and the melting-curve—thermometer pressure at $T_c(P)$, were least-squares-fitted using the expression

$$\Delta P_{\rm MC} \equiv P_{\rm MC}(T_c) - P_A = \sum_{l=1}^{4} b_l (P_A - P)^l . \quad (5)$$

The best-fit parameters, with all pressures in bars, are

$$b_1 = 0.319\,329\,93 \times 10^{-3} ,$$

$$b_2 = 0.274\,226\,06 \times 10^{-4} ,$$

$$b_3 = -0.593\,232\,02 \times 10^{-6} ,$$

$$b_4 = 0.239\,372\,50 \times 10^{-7} .$$

The smoothed results are plotted in Fig. 9 and listed in Table III. Note the curious result that at $P=0$, $\Delta P_{\rm MC} = 52.56$ mbar, i.e., $T_c(P=0) \approx T_S$. The deviations from the best fit are plotted in Fig. 10. The scatter in the data is generally less than 50 μbar, but systematic deviations from the fit are as large at 0.2 mbar. It should be noted that the accuracy of the results described by Eq. (5) depends only on the accuracy of the pressure calibrations (Sec. II C) and on the precision with which the superfluid transition could be located; these data are completely in-

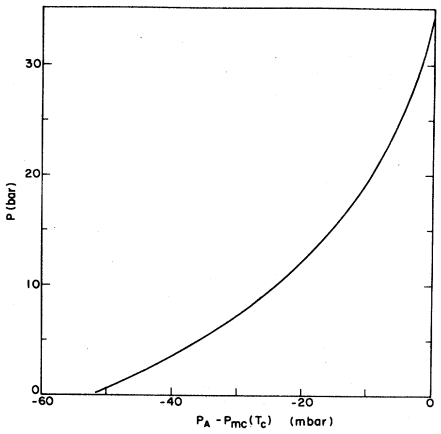

FIG. 9. Melting-curve—thermometer pressure at T_c as a function of sample pressure. The smooth curve was drawn using Eq. (5).

TABLE III. Pressure-temperature coordinates for the transition between normal and superfluid ^{3}He. The smoothed values were computed using Eqs. (3) and (5).

P (bars)	$\Delta P_{\rm MC}$ (mbar)	T_c (mK)
0	52.560	1.080
1	48.712	1.219
2	45.119	1.343
3	41.767	1.457
4	38.641	1.560
5	35.725	1.654
6	33.007	1.741
7	30.474	1.820
8	28.113	1.893
9	25.913	1.961
10	23.862	2.023
11	21.949	2.080
12	20.164	2.133
13	18.499	2.182
14	16.942	2.228
15	15.488	2.270
16	14.126	2.310
17	12.851	2.347
18	11.656	2.381
19	10.533	2.413
20	9.479	2.443
21	8.488	2.471
22	7.555	2.497
23	6.677	2.522
24	5.850	2.545
25	5.072	2.567
26	4.341	2.588
27	3.655	2.607
28	3.013	2.625
29	2.415	2.641
30	1.861	2.657
31	1.352	2.671
32	0.890	2.684
33	0.475	2.695
34	0.111	2.705
34.338	0.000	2.708

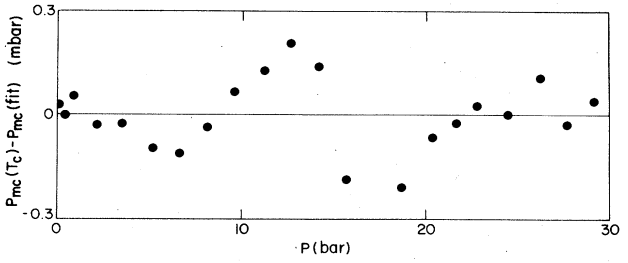

FIG. 10. Deviations of the melting-curve—thermometer pressure measured at $T_c(P)$ from the best-fit curve described by Eq. (5).

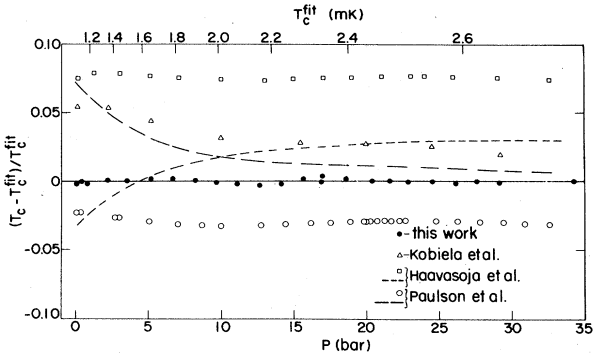

FIG. 12. Deviations from the transition line between normal and superfluid ^{3}He determined by Eqs. (3) and (5). Details are given in the text.

dependent of temperature scale.

Equation (3) in conjunction with Eq. (5) determines $T_c(P)$. These smoothed transition temperatures are listed in Table III and are also plotted as a function of sample pressure in Fig. 11. The differences between the measured and smoothed values of $P_{MC}(T_c)$ (Fig. 10) converted to relative temperature differences are shown in Fig. 12. Over the entire pressure range the deviations (solid circles) are less than 0.5%.

Comparison with several other determinations of $T_c(P)$ is also made in Fig. 12. The triangles are the very recent measurements of Kobiela *et al.*,[21] again based on the melting-curve calibration of Halperin *et al.*,[6] but using $T_A=2.752$ mK. These results, therefore, should lie uniformly 1.6% higher than ours. At the higher pressures the differences between the two sets of measurements do tend toward this value, but at the lowest pressures there is an additional difference of 3.8%. Quantitatively consistent with this large discrepancy, Kobiela *et al.* observe that $T_c(P=0)$ is 37 μK higher than T_S, while we find $T_c(P=0)$ is less than but very nearly equal to T_S. The problem could be explained if there were significant self-heating in our LCMN thermometer or in their melting-curve thermometer. However, checks on our thermometer indicated that the amount of self-heating was small, and self-heating in melting-curve thermometers is generally not a problem. We note that Osheroff[27] has also observed that $T_c(P=0)\lesssim T_S$, but his two determinations were separated in time by a period of several days.

The short-dashed curve shows the smoothed T_c's of Haavasoja *et al.*[28] determined using a LCMN thermometer, with the Δ (-0.12 mK) extracted from a calibration against a platinum NMR thermometer. The long-dashed curve shows the results of Paulson *et al.*,[29] again measured using a LCMN thermometer. Their Δ ($+0.10$ mK) was estimated using the condition that the zero-sound attenuation be proportional to T^2 for temperatures high compared to T_c. Both dashed curves depart from the reference line in a qualitatively similar manner, but with opposite sign. This suggests that the deviations, which become largest at the lowest temperature, are associated with the Δ's. The open squares and circles are the two respective sets of data replotted with $\Delta=0$. To quite high accuracy, both T^* scales are proportional to the Cornell scale. Assuming no significant errors in our mapping of the Cornell melting-curve scale onto the superfluid phase diagram, and assuming also that the Cornell scale is accurately proportional to the thermodynamic temperature, it must be concluded that both Δ's are essentially zero. Furthermore, if our estimate of $T_A=2.708$ mK is correct, then the $T=T^*$ scale of Haavasoja *et al.* is too large by 7.5% and the $T=T^*$ scale of Paulson *et al.* is too small by 3%. These numbers can be compared with the estimates of the absolute accuracy of 5% and 2%, respectively.

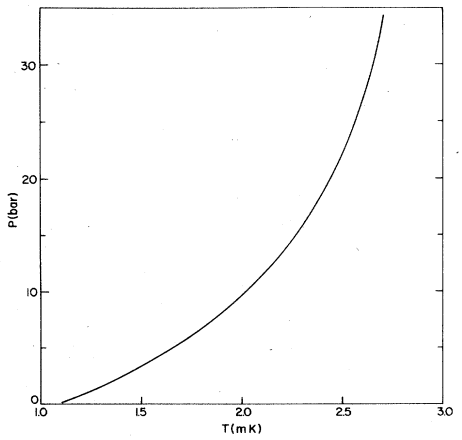

FIG. 11. Transition line between normal and superfluid ^{3}He based on Eqs. (3) and (5).

ACKNOWLEDGMENTS

I would like to thank D. D. Osheroff, M. A. Paalanen, J. M. Parpia, R. C. Richardson, and W. O. Sprenger for helpful discussions and comments. I am also grateful to P. A. Busch for his technical assistance.

[1]R. A. Scribner and D. E. Adams, in *Temperature,* edited by H. H. Plumb (Instrument Society of America, Pittsburgh, Pennsylvania, 1972), Vol. 4, Pt. 1, p. 37.
[2]D. S. Greywall, Phys. Rev. B **27**, 2747 (1983).
[3]D. S. Greywall, Phys. Rev. B **29**, 4933 (1984).
[4]D. S. Greywall and P. A. Busch, J. Low Temp. Phys. **46**, 451 (1982).
[5]J. H. Colwell, W. E. Fogle, and R. J. Soulen, Jr., in *Proceedings of the 17th International Conference on Low Temperature Physics,* edited by U. Eckern, A. Schmid, W. Weber, and H. Wühl (North-Holland, Amsterdam, 1984), Pt. 1, p. 395; and private communication.
[6]W. P. Halperin, F. B. Rasmussen, C. N. Archie, and R. C. Richardson, J. Low Temp. Phys. **31**, 617 (1978).
[7]Materials Preparation Center, Ames Laboratory, Iowa State University, Ames, IA 50011.
[8]Materials Research Corp. Orangeburg, NY 10962. The copper had a nominal purity of 99.999%. We note that the electrical resistivity ratio varied significantly from batch to batch. Samples from two batches annealed simultaneously (930 °C, 3 d, ^{4}He atmosphere) yielded ratios of 500 and 1350.
[9]First, a very thin layer of copper was plated on the rods using a cyanide bath. This layer protected the small amount of exposed cadmium (in the seams between the copper wires and $PrNi_5$) from the acid bath used to complete the plating. Various samples of electroplated copper had resistivity ratios between 50 and 100.
[10]During the welding operation the $PrNi_5$ rods were submerged in a bath of liquid argon.
[11]J. M. Parpia, W. P. Kirk, P. S. Kobiela, T. L. Rhodes, Z. Olejniczak, and G. N. Parker (unpublished).
[12]W. O. Sprenger (unpublished).
[13]E. I. Dupont de Nemours, Polymer Products Department, Wilmington, DE 19898, type SP-22.
[14]The annealed (180 °C, 6 h, ^{4}He atmosphere) piece of tin (99.9999% pure), before soldering, had a resistivity ratio in excess of 20 000. The tin heat switch is similar in design to one used by D. D. Osheroff.
[15]R. M. Mueller, C. Buchal, H. R. Folle, M. Kubota, and F. Pobell, Cryogenics **20**, 395 (1980).
[16]Except for the mounting arrangement of the coils, this thermometer is very similar to the LCMN thermometer described in Ref. 4.
[17]Vacuum Metallurgical Co., Tokyo, Japan.
[18]P. A. Busch, S. P. Cheston, and D. S. Greywall, Cryogenics **24**, 445 (1984).
[19]72 at. % silver, 28 at. % copper. The soldering was done in an oven, under a ^{4}He atmosphere and as quickly as possible. On test pieces of high-purity copper wire lapped and soldered together we maintained resistivity ratios greater than 1100.
[20]O. Avenel, M. Bernier, D. Bloyet, P. Piejus, E. Varaquaux, and C. Vibet, in *Proceedings of LT-14 (Otaniemi, Finland),* edited by M. Krusius and M. Vuorio (North-Holland, Amsterdam, 1975), Vol. 4, p. 64.
[21]P. S. Kobiela, Z. Olejniczak, W. P. Kirk, and J. M. Parpia, in *Proceedings of the 17th International Conference on Low Temperature Physics,* Ref. 5, Pt. II, p. 1173.
[22]D. D. Osheroff and C. Yu, Phys. Lett. **77A** 458 (1980).
[23]J. C. Wheatley, Rev. Mod. Phys. **47**, 415 (1975).
[24]R. C. Richardson, Physica **90B**, 47 (1977).
[25]The solution of the three equations gives

$$\Delta = [NT_3(T_2-T_1)-T_2(T_3-T_1)] \times [N(T_2-T_1)-(T_3-T_1)]^{-1} ,$$

with $N \equiv (X_1-X_3)/(X_1-X_2)$. Numerically, $\Delta = 0.286$ mK.
[26]D. D. Osheroff and R. C. Richardson (unpublished).
[27]D. D. Osheroff (private communication).
[28]T. Haavasoja, Ph.D. thesis, Helsinki University of Technology, 1980; T. A. Alvesalo, T. Haavasoja, and M. T. Manninen, J. Low Temp. Phys. **45**, 373 (1981); T. A. Alvesalo, T. Haavasoja, M. T. Manninen, and A. T. Soinne, Phys. Rev. Lett. **44**, 1076 (1980).
[29]D. N. Paulson, M. Krusius, J. C. Wheatley, R. S. Safrata, M. Koláč, T. Těthal, K. Svec, and J. Matas, J. Low Temp. Phys. **34**, 63 (1979); **36**, 721(E) (1979).